

# Identification of Ubiquinol Binding Motifs at the $Q_o$ -site of the Cytochrome $bc_1$ Complex (Supplementary material)

Angela M. Barragan,<sup>†,‡</sup> Antony R. Crofts,<sup>¶,§</sup> Klaus Schulten,<sup>†,‡</sup> and Ilia A.  
Solov'yov<sup>\*,||</sup>

*Department of Physics, University of Illinois at Urbana–Champaign, 1110 W. Green Street,  
Urbana, IL 61801, USA, Beckman Institute for Advanced Science and Technology,  
University of Illinois at Urbana–Champaign, 405 N. Mathews Ave, Urbana, IL 61801,  
USA, Department of Biochemistry, University of Illinois Urbana–Champaign, 600 S.  
Mathews Ave, Urbana, IL 61801, USA, Center for Biophysics and Computational Biology,  
University of Illinois Urbana–Champaign, 607 S. Mathews Ave, Urbana, IL 61801, USA,  
and Department of Physics, Chemistry and Pharmacy, University of Southern Denmark,  
Campusvej 55, DK-5230 Odense M, Denmark*

E-mail: [ilia@sdu.dk](mailto:ilia@sdu.dk)

---

\*To whom correspondence should be addressed

<sup>†</sup>University of Illinois at Urbana–Champaign, Department of Physics

<sup>‡</sup>University of Illinois at Urbana–Champaign, Beckman Institute

<sup>¶</sup>University of Illinois at Urbana–Champaign, Department of Biochemistry

<sup>§</sup>University of Illinois at Urbana–Champaign, Center for Biophysics and Computational Biology

<sup>||</sup>University of Southern Denmark

## Q<sub>o</sub>-site binding motifs: experimental insights

Several different scenarios have been suggested for the chemical specificity of the QH<sub>2</sub> ··· H156 hydrogen bonding. The reduction of ISP involves transfer of both an electron and a proton, and such proton-coupled electron transfers can follow different pathways. The actual protonation state of H156 greatly impacts the initial reaction at the Q<sub>o</sub>-site because it determines which residue acts as H-bond donor, and hence the probable sequence of transfer. A substantial literature has considered different sequences,<sup>1-7</sup> - proton-first-then-electron, electron-then-proton, concerted, etc., - with important consequences for understanding reaction mechanisms in the many different enzymes in which they occur. In the *bc*<sub>1</sub> complex, each of the partial reactions involving semiquinone species occurs by a different mechanism, and the underlying reaction mechanisms have, therefore, attracted much attention. In general, the hydrogen bonding between two dissociable groups is determined by their *pK* values. These can be perturbed by the protein environment, but are known to good approximation for the species involved here;<sup>1,3,8</sup> *pK*<sub>ox1</sub> associated with H156 is 7.6 in the subunit isolated from wildtype,<sup>9,10</sup> and *pK* for dissociation of QH<sub>2</sub> to QH• is ≥11.5. Furthermore, the *pK* of H156 has been changed by mutagenesis of key residues, allowing exploration of the importance of this parameter in modulation of the properties of the first electron transfer in the *bc*<sub>1</sub> complex.<sup>2,3,11,12</sup> The reaction shows strong pH dependence in the range about the *pK*<sub>ox1</sub> of H156, but with a titration curve (apparent *pK* ~6.65 determined kinetically)<sup>1,11</sup> displaced by about 1 pH unit from the value (*pK*<sub>ox1</sub> ~7.6) measured in the isolated subunit. Since the displaced value tracks changes in *pK*<sub>ox1</sub> in mutant strains (Fig. S1),<sup>2,11</sup> it is clear that both reflect the *pK* of H156, with the displacement likely associated with the work involved in forming a hydrogen bond. Since rates are maximal at pH values above the *pK*, it is also clear that they reflect involvement of the dissociated form in formation of the productive reaction complex. However, significant activity is observed at environmental pH well below the *pK*, suggesting that electron transfer can occur even with H156 in the protonated form.<sup>1,2,6</sup> To establish the binding mode of QH<sub>2</sub> at the Q<sub>o</sub>-site, it is, therefore,

necessary to consider both protonation states of H156. In addition, one needs to identify other key residues that contribute to the binding of the QH<sub>2</sub> substrate molecule within the bc<sub>1</sub> complex. Particularly important, in this respect, is the inclusion of all charged and polar residues that can potentially contribute to substrate binding at the Q<sub>o</sub>-site, as these residues can impact critically the rate of electron and proton transfers.

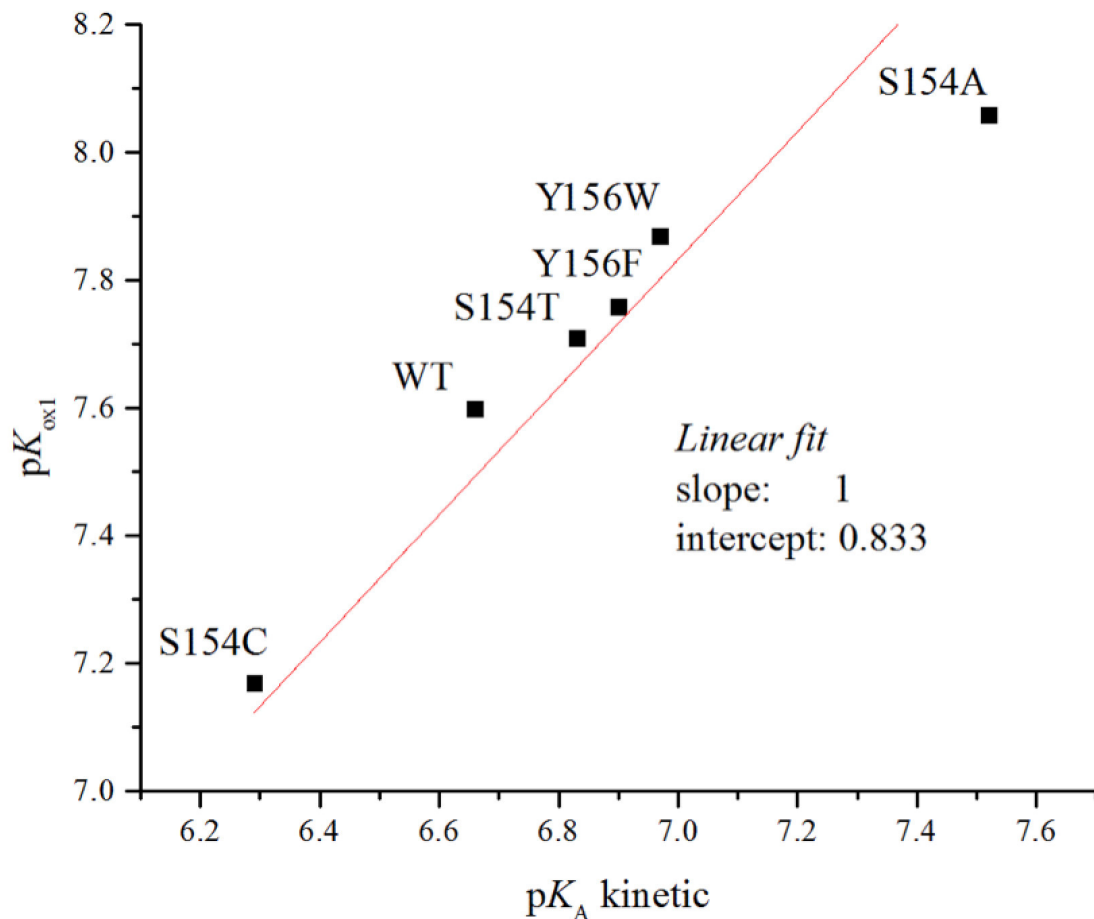


Figure S1: **Correlation between  $pK_{ox1}$  and  $pK_A$ .** Correlation between the  $pK_A$  value measured kinetically, which reflects the occupancy of the reaction complex, and the  $pK_{ox1}$  of H156, determined from the pH dependence of the redox potential in different mutant strains.

## Protonated H156 at the Q<sub>o</sub>-site (Model I)

### Membrane equilibration

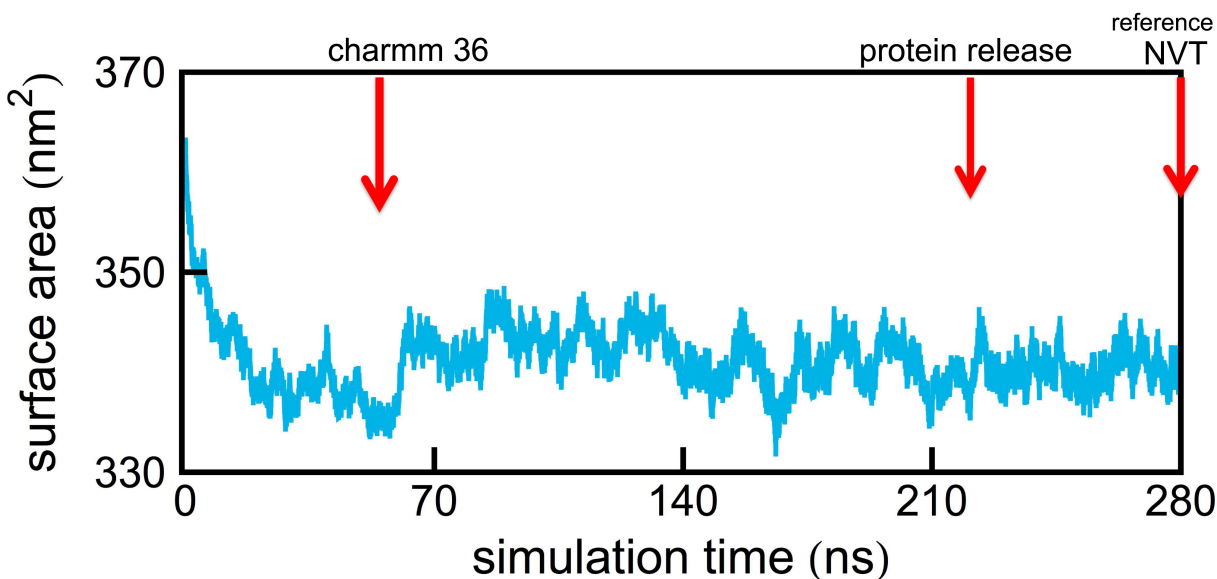


Figure S2: **Lipid bilayer equilibration.** Time evolution of the surface area of the lipid bilayer, calculated during the Model I equilibration. The first 60 ns were simulated with a combination of CHARMM 22 and 27 force fields, as done in,<sup>13</sup> while CHARMM 36 was used beyond 60 ns (point indicated with an arrow). The proteins of the *bc*<sub>1</sub> complex were constrained to the configuration of the crystal structure and subsequently released after 220 ns, as also indicated by a vertical arrow. MD simulations beyond 280 ns were continued in the NVT ensemble, and the configuration of the system at the 280 ns simulation instance was used as a reference structure in further analysis.

## $bc_1$ complex equilibration

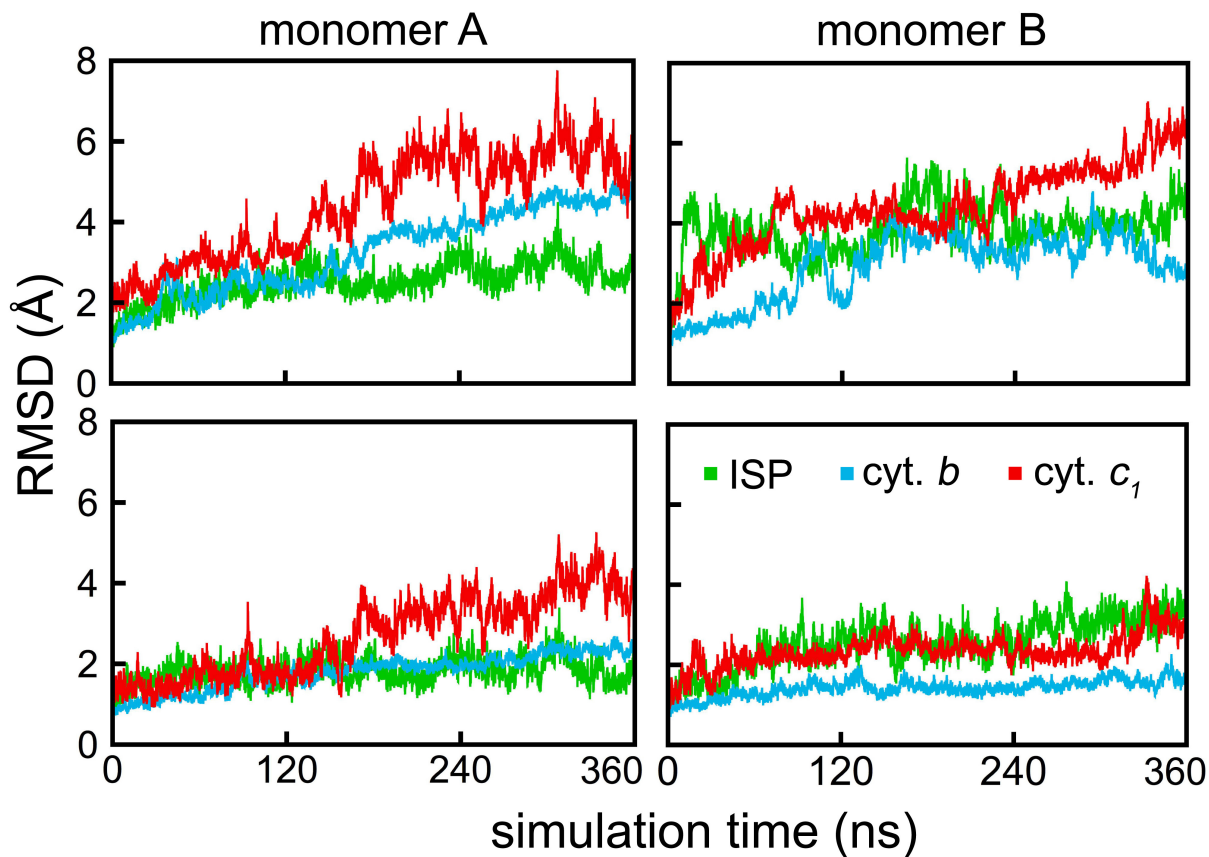


Figure S3: **Equilibration of the  $bc_1$  complex.** RMSD values calculated for the protein subunits of the two monomers (A and B) of the  $bc_1$  complex in case of Model I (Fig. 1). Upper panels: RMSD calculated for all atoms of the protein's backbone. Lower panels: RMSD computed only for the atoms of the secondary structure motifs that exclude bridges, coils and turns. All RMSD plots were computed with respect to the reference structure noted in Fig. S2.

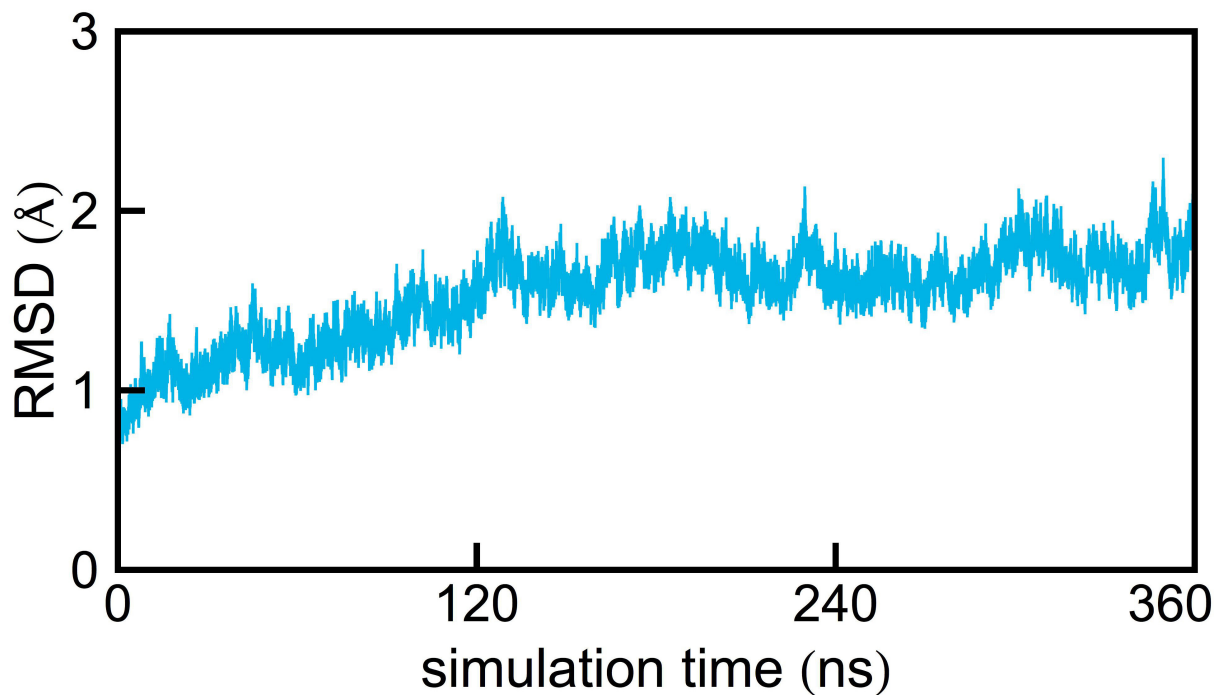


Figure S4: **Equilibration of intermembrane helices.** Shown are RMSD values calculated for the atoms of the transmembrane helices of the  $bc_1$  complex in case of Model I. RMSD values were computed with respect to the reference structure noted in Fig. S2.

## Deprotonated H156 at the $Q_o$ -site (Model II)

### Membrane equilibration

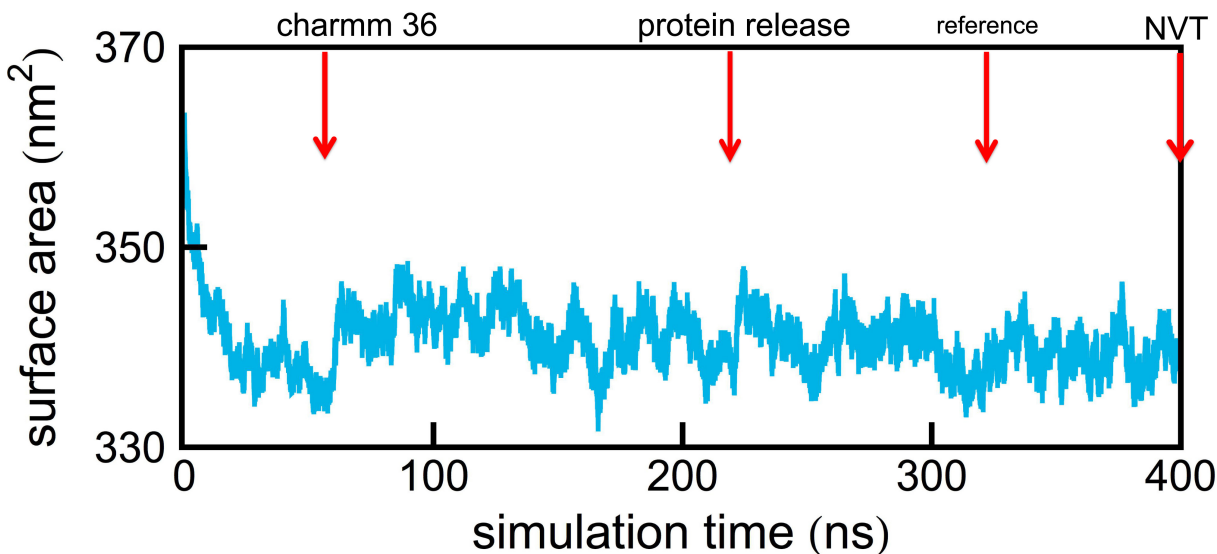


Figure S5: **Lipid bilayer equilibration.** Surface area of the lipid bilayer as a function of simulation time, calculated during the equilibration of Model II. The  $bc_1$  complex proteins were released after 220 ns; up until this point the simulations of Model I and Model II were carried out identically. RMSD value calculations of the  $bc_1$  complex protein subunits and the hydrogen bonding network analysis were performed with respect to the configuration of the system at 310 ns, as indicated by a vertical arrow marked “reference”. MD simulations beyond 400 ns were carried out in the NVT ensemble.

## $bc_1$ complex equilibration

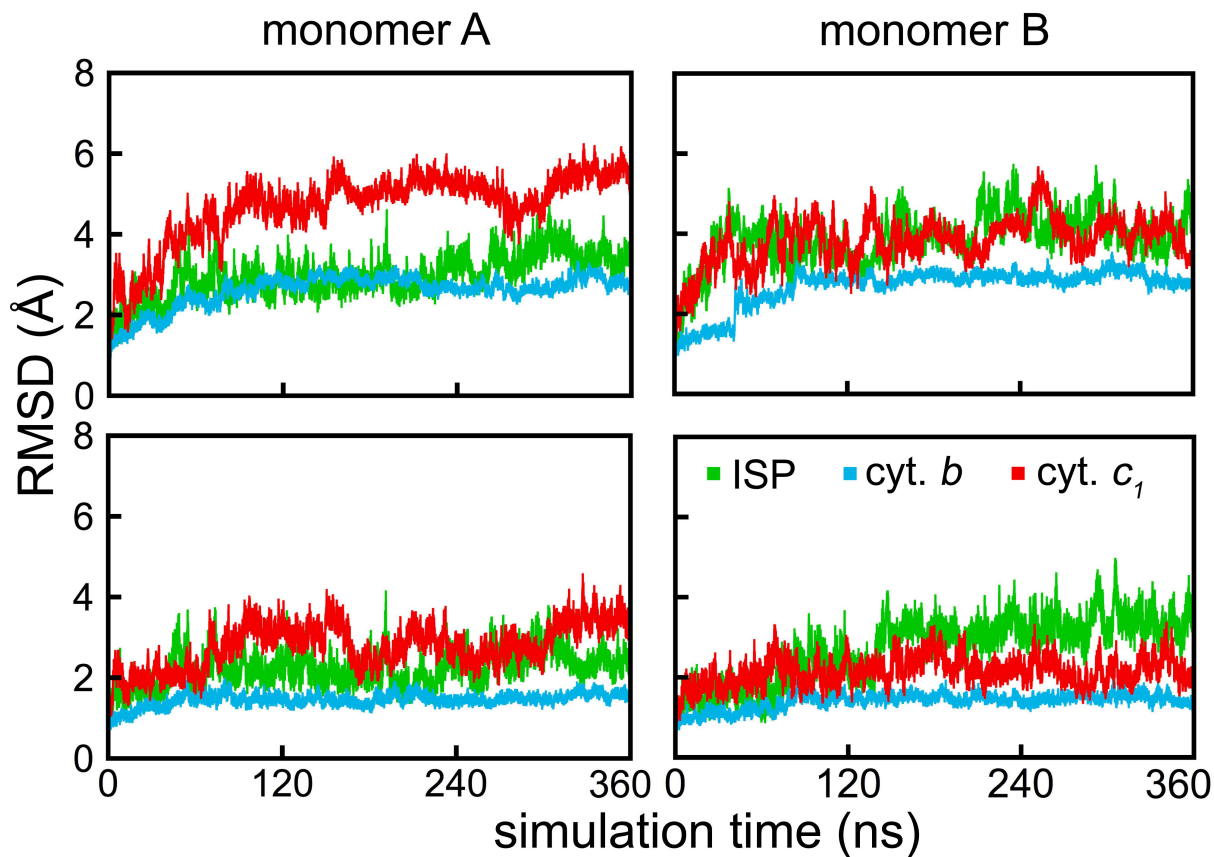


Figure S6: **Equilibration of  $bc_1$  complex.** RMSD values calculated for the protein subunits of the two monomers (A and B) of the  $bc_1$  complex in case of Model II (Fig. 1). Upper panels: RMSD calculated for all atoms of the protein's backbone. Lower panels: RMSD computed only for the atoms of the secondary structure motifs that exclude bridges, coils and turns. All RMSD plots are computed with respect to the reference structure noted in Fig. S5.

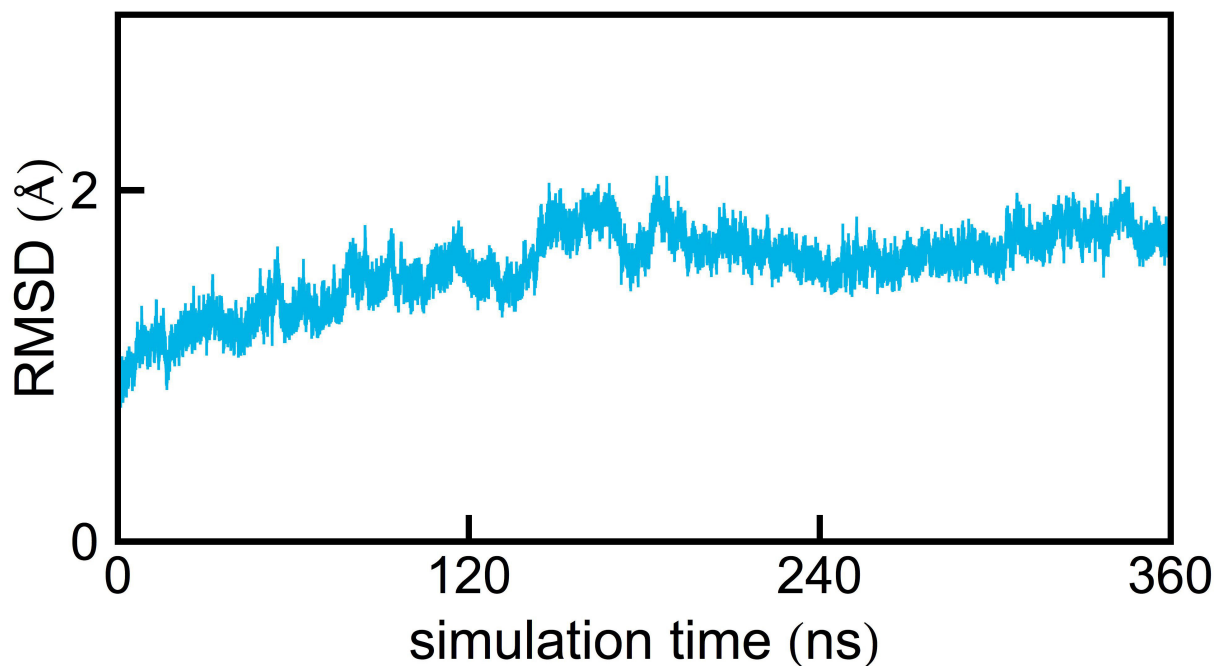


Figure S7: **Equilibration of intermembrane helices.** Shown are RMSD values calculated for the atoms of the transmembrane helices of the  $bc_1$  complex in case of Model II. The RMSD values were computed with respect to the reference structure obtained after 310 ns of membrane and protein equilibration noted in Fig. S5.

## Quantum chemistry study of Q<sub>o</sub>-site quinol binding

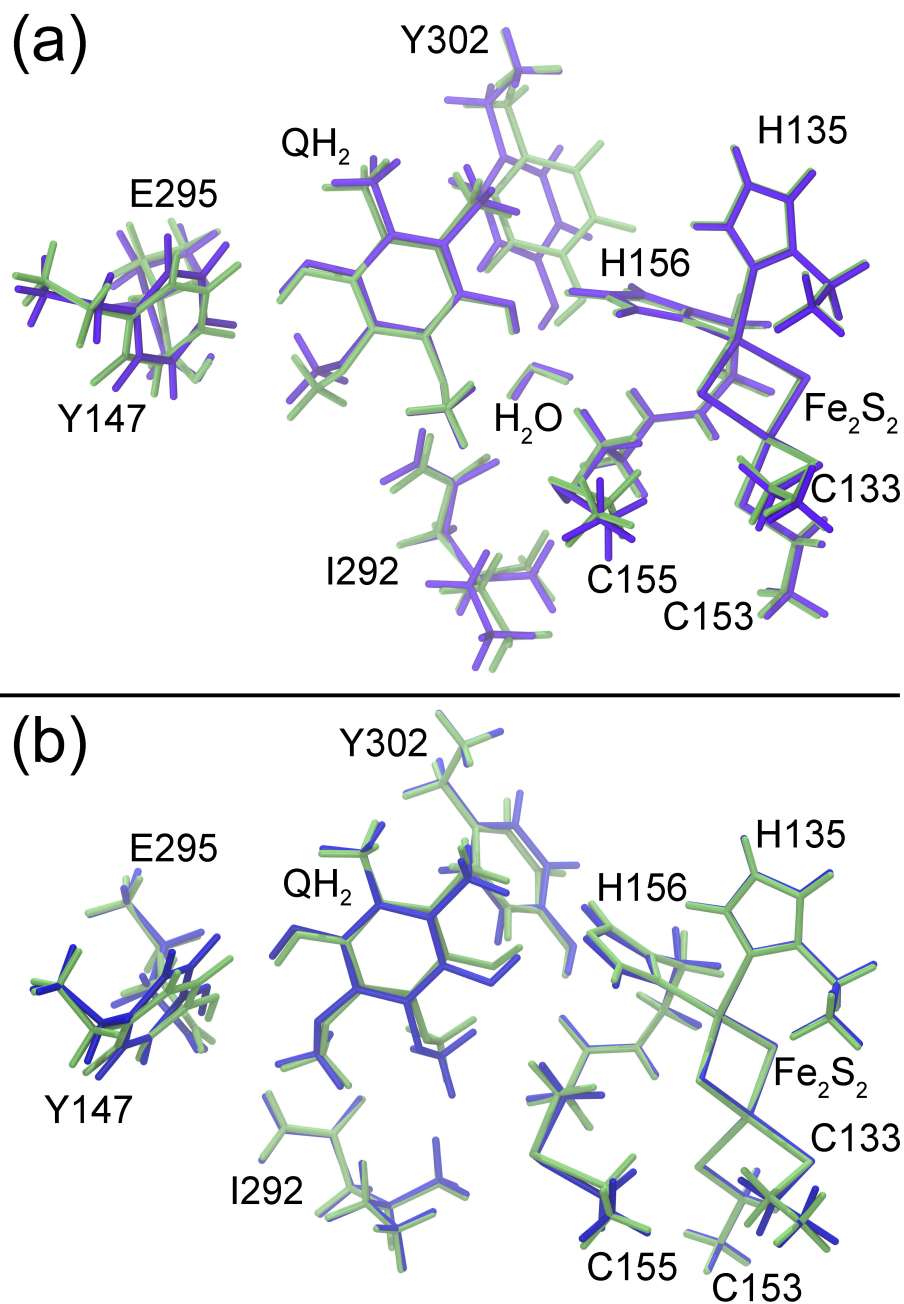


Figure S8: **Comparison of quantum chemical optimizations of the Q<sub>o</sub>-site.** Shown are aligned optimized structures of the Q<sub>o</sub>-site for Model I (a) and Model II (b) obtained using the B3LYP/6-311G(d) (lime) and B3LYP/6-311+G(d) (blue) methods. The structures were aligned to minimize the relative RMSD value which equals 0.37 Å and 0.33 Å in the case of Model I and Model II, respectively.

## Supporting Files

The CHARMM topology file, `top_H156.inp`, obtained for the MD simulations performed in this study for Model II, is included with this supporting material. This topology file includes the topology of the deprotonated H156 residue together with the Fe<sub>2</sub>S<sub>2</sub> cluster and the ligating residues C133, C153, H135. It includes the charges fitted to the electrostatic potential (ESP), calculated using the B3LYP/6-31G(d) model chemistry.

## References

- (1) Hong, S.; Ugulava, N.; Guergova-Kuras, M.; Crofts, A. R. The Energy Landscape for Ubihydroquinone Oxidation at the Q<sub>o</sub> Site of the bc<sub>1</sub> Complex in Rhodobacter Sphaeroides. *J. Biol. Chem.* **1999**, *274*, 33931–33944.
- (2) Guergova-Kuras, M.; Kuras, R.; Ugulava, N.; Hadad, I.; Crofts, A. R. Specific Mutagenesis of the Rieske Iron-sulfur Protein in Rhodobacter Sphaeroides Shows that both the Thermodynamic Gradient and the pK of the Oxidized form Determine the Rate of Quinol Oxidation by the bc<sub>1</sub> Complex. *Biochemistry* **2000**, *39*, 7436–7444.
- (3) Zu, Y.; Couture, M. M.-J.; Kolling, D. R.; Crofts, A. R.; Eltis, L. D.; Fee, J. A.; Hirst, J. Reduction Potentials of Rieske Clusters: Importance of the Coupling Between Oxidation State and Histidine Protonation State. *Biochemistry* **2003**, *42*, 12400–12408.
- (4) Hammes-Schiffer, S. Current Theoretical Challenges in Proton–Coupled Electron Transfer: Electron–Proton Nonadiabaticity, Proton Relays, and Ultrafast Dynamics. *J. Phys. Chem. Lett.* **2011**, *2*, 1410–1416.
- (5) Hammes-Schiffer, S. Catalytic Efficiency of Enzymes: A Theoretical Analysis. *Biochemistry* **2013**, *52*, 2012–2020.
- (6) Brandt, U.; Okun, J. G. Role of Deprotonation Events in Ubihydroquinone: Cy-

- tochrome c Oxidoreductase from Bovine Heart and Yeast Mitochondria. *Biochemistry* **1997**, *36*, 11234–11240.
- (7) Hammes-Schiffer, S.; Soudackov, A. V. Proton–Coupled Electron Transfer in Solution, Proteins, and Electrochemistry. *J. Phys. Chem. B* **2008**, *112*, 14108–14123.
- (8) Leggate, E. J.; Hirst, J. Roles of the Disulfide Bond and Adjacent Residues in Determining the Reduction Potentials and Stabilities of Respiratory-type Rieske Clusters. *Biochemistry* **2005**, *44*, 7048–7058.
- (9) Link, T. A. Two pK Values of the Oxidised Rieske [2Fe-2S] Cluster Observed by CD Spectroscopy. *Biochim. Biophys. Acta – Bioener.* **1994**, *1185*, 81–84.
- (10) Rich, P. R.; Bendall, D. S. The Kinetics and Thermodynamics of the Reduction of Cytochrome *c* by Substituted *p*-benzoquinols in Solution. *Biochim. Biophys. Acta – Bioener.* **1980**, *592*, 506–518.
- (11) Lhee, S.; Kolling, D. R.; Nair, S. K.; Dikanov, S. A.; Crofts, A. R. Modifications of Protein Environment of the [2Fe-2S] Cluster of the bc<sub>1</sub> Complex: Effects on the Biophysical Properties of the Rieske Iron-sulfur Protein and on the Kinetics of the Complex. *J. Biol. Chem.* **2010**, *285*, 9233–9248.
- (12) Kolling, D. J.; Brunzelle, J. S.; Lhee, S.; Crofts, A. R.; Nair, S. K. Atomic Resolution Structures of Rieske Iron-sulfur Protein: Role of Hydrogen Bonds in Tuning the Redox Potential of Iron-sulfur Clusters. *Structure* **2007**, *15*, 29–38.
- (13) Postila, P. A.; Kaszuba, K.; Sarewicz, M.; Osyczka, A.; Vattulainen, I.; Róg, T. Key Role of Water in Proton Transfer at the Q<sub>o</sub>-site of the Cytochrome bc<sub>1</sub> Complex Predicted by Atomistic Molecular Dynamics Simulations. *Biochim. Biophys. Acta – Bioener.* **2013**, *1827*, 761–768.